11576 *Inorg. Chem.* **2009**, *48*, 11576–11585
DOI: 10.1021/ic901329z

Inorganic Chemistry
Article

Aryl-Containing Chelates and Amine Debenzylation to Afford 1,3-Di-2-pyridyl-2-azaallyl (smif): Structures of $\{\kappa$-C,N,N$^{py}_2$-(2-pyridylmethyl)$_2$N(CH$_2$(4-^{t}Bu-phenyl-2-yl))$\}$FeBr and (smif)CrN(TMS)$_2$

Brenda A. Frazier, Peter T. Wolczanski,* and Emil B. Lobkovsky

Department of Chemistry & Chemical Biology, Baker Laboratory, Cornell University, Ithaca, New York 14853

Received July 9, 2009

Aryl-bromide ligand precursors have been prepared with the potential to afford tetradentate chelates (2-pyridylmethyl)$_{3-x}$N(CH$_2$-2-Aryl)$_x$ (x = 1, 2) containing metal-aryl linkages that promise to impart stronger fields about first row transition metals. Oxidative addition to Ni(COD)$_2$ afforded two diamagnetic Ni(II) complexes, $\{\kappa$-C,N,N^{py}-(2-pyridylmethyl)N(CH$_2$(4-^{t}Bu-phenyl-2-yl))(CH$_2$(4-^{t}Bu-phenyl-2-Br))$\}$NiBr (**1**-Ni) and $\{(\kappa$-C,N,N$^{py}_2$-(2-pyridylmethyl)$_2$N-(CH$_2$(4-^{t}Bu-phenyl-2-yl))$\}$NiBr (**2**-Ni) in 96% and 67% yield, respectively. Extending these synthetic efforts to iron provided $\{\kappa$-C,N,N$^{py}_2$-(2-pyridylmethyl)$_2$N(CH$_2$(4-^{t}Bu-phenyl-2-yl))$\}$FeBr (**2**-Fe, X-ray) in 91% yield via reduction of an adduct, $\{\kappa$-N,N$^{py}_2$-(2-pyridylmethyl)$_2$N(CH$_2$(4-^{t}Bu-phenyl-2-Br))$\}$FeBr$_2$ (**3**-Fe). 5-Coordinate **2**-Fe possessed a pseudo-tbp structure, and SQUID magnetometry showed it to be S = 2 with significant zero field splitting (ZFS). **2**-Fe was initially prepared via oxidative addition to Fe$\{$N(TMS)$_2\}_2$(THF) upon disproportionation to "Fe(0)" and 2 Fe$\{$N(TMS)$_2\}_3$, but when this approach was attempted with Cr$\{$N(TMS)$_2\}_2$(THF)$_2$, the azaallyl complex $\{\kappa$-N,N$^{py}_2$-1,3-dipyridyl-2-azaallyl$\}$CrN(TMS)$_2$ ((smif)CrN(TMS)$_2$, **4**-Cr, X-ray), formed instead (>50%) via amine debenzylation. An alternative route consisting of addition of 1,3-di-2-pyridyl-2-azapropene to Cr$\{$N(TMS)$_2\}_2$(THF)$_2$ afforded **4**-Cr in 74% yield. Pseudo-square planar **4**-Cr was also S = 2 (SQUID) with marked ZFS. The dipyridylazaallyl ligand "smif" imparts a remarkable optical density to **4**-Cr via intraligand bands at 675 nm ($\varepsilon \sim 15\,000$ M^{-1}cm^{-1}) and 396 nm ($\varepsilon \sim 27\,000$ M^{-1}cm^{-1}). The effective fields of the chelate complexes are discussed, and a comparison of smif to isoelectronic NHC ligands is given.

Introduction

Electronic features that distinguish the structure and reactivity of second row transition metals from their third row congeners have been the focus of recent activity in these laboratories[1−8] and others.[9−17] Greater $(n + 1)$s/nd$_{z^2}$ mixing in the third row tends to decrease the density of states (DOS) in 5d complexes, whereas lesser mixing in the 4d elements results in a relatively greater DOS. As a consequence, the path from reactant to product for a second row transition metal species may utilize electronic surfaces other than those of the respective ground states, thereby facilitating chemical

*To whom correspondence should be addressed. E-mail: ptw2@cornell.edu.

(1) Hirsekorn, K. F.; Hulley, E. B.; Wolczanski, P. T.; Cundari, T. R. *J. Am. Chem. Soc.* **2008**, *130*, 1183–1196.
(2) Kuiper, D. S.; Douthwaite, R. E.; Mayol, A.-R.; Wolczanski, P. T.; Lobkovsky, E. B.; Cundari, T. R.; Lam, O. P.; Meyer, K. *Inorg. Chem.* **2008**, *47*, 7139–7153.
(3) Kuiper, D. S.; Wolczanski, P. T.; Lobkovsky, E. B.; Cundari, T. R. *J. Am. Chem. Soc.* **2008**, *130*, 12931–12943.
(4) Kuiper, D. S.; Wolczanski, P. T.; Lobkovsky, E. B.; Cundari, T. R. *Inorg. Chem.* **2008**, *47*, 10542–10553.
(5) Rosenfeld, D. C.; Wolczanski, P. T.; Barakat, K. A.; Buda, C.; Cundari, T. R.; Schroeder, F. C.; Lobkovsky, E. B. *Inorg. Chem.* **2007**, *46*, 9715–9735.
(6) Veige, A. S.; Slaughter, L. M.; Lobkovsky, E. B.; Wolczanski, P. T.; Matsunaga, N.; Decker, S. A.; Cundari, T. R. *Inorg. Chem.* **2003**, *42*, 6204–6224.
(7) Rosenfeld, D. C.; Kuiper, D. S.; Lobkovsky, E. B.; Wolczanski, P. T. *Polyhedron* **2006**, *25*, 251–258.
(8) Wolczanski, P. T. *Chem. Commun.* **2009**, 740–757.
(9) (a) Poli, R. *J. Organomet. Chem.* **2004**, *689*, 4291–4304. (b) Poli, R. *Acc. Chem. Res.* **1997**, *30*, 1861–1866.
(10) Matsunaga, N.; Koseki, S. *Rev. Comput. Chem* **2004**, *20*, 101–152.
(11) Carreon-Macedo, J.; Harvey, J. N.; Poli, R. *Eur. J. Inorg. Chem.* **2005**, *12*, 2999–3008.
(12) Poli, R.; Cacelli, I. *Eur. J. Inorg. Chem.* **2005**, *12*, 2324–2331.
(13) (a) Petit, A.; Richard, P.; Cacelli, I.; Poli, R. *Chem.—Eur. J.* **2006**, *12*, 813–823. (b) Smith, K. M.; Poli, R.; Harvey, J. N. *Chem.—Eur. J.* **2001**, *7*, 1679–1690.
(14) (a) Schrock, R. R.; Seidel, S. W.; Mosch-Zanetti, N. C.; Shih, K. Y.; O'Donoghue, M. B.; Davis, W. M.; Reiff, W. M. *J. Am. Chem. Soc.* **1997**, *119*, 11876–11893. (b) Schrock, R. R.; Seidel, S. W.; MoschZanetti, N. C.; Dobbs, D. A.; Shih, K. Y.; Davis, W. M. *Organometallics* **1997**, *16*, 5195–5208.
(15) (a) Buccella, D.; Tanski, J. M.; Parkin, G. *Organometallics* **2007**, *26*, 3275–3278. (b) Buccella, D.; Parkin, G. *J. Am. Chem. Soc.* **2006**, *128*, 16358–16364. (c) Churchill, D. G.; Janak, K. E.; Wittenberg, J. S.; Parkin, G. *J. Am. Chem. Soc.* **2003**, *125*, 1403–1420.
(16) (a) Fan, L.; Parkin, S.; Ozerov, O. V. *J. Am. Chem. Soc.* **2005**, *127*, 16772–16773. (b) Weng, W.; Guo, C. Y.; Moura, C.; Yang, L.; Foxman, B. M.; Ozerov, O. V. *Organometallics* **2005**, *24*, 3487–3499.
(17) Soo, H. S.; Figueroa, J. S.; Cummins, C. C. *J. Am. Chem. Soc.* **2004**, *126*, 11370–11376.

Published on Web 09/21/2009

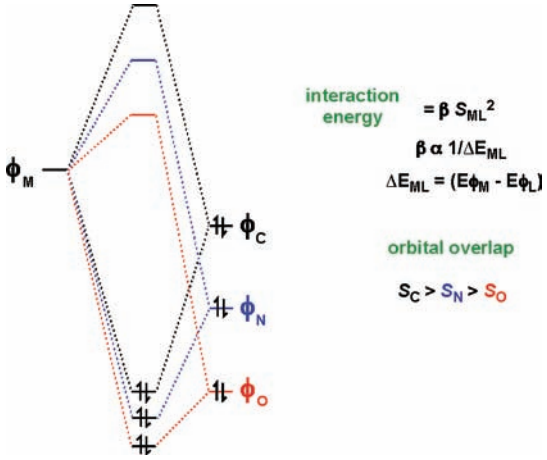

Figure 1. Angular overlap arguments show that both the interaction energy and orbital overlap favor C-based over N- and O-based ligands in terms of field strength.

reactivity.[1] Particular coordination geometries may also be impacted by $(n + 1)s/nd_{z^2}$ mixing; 4-coordinate Mo(IV) derivatives have been shown to be pseudo-tetrahedral, while related W complexes tend toward square planar.[2,17]

In principle, and certainly from a spectroscopic standpoint,[18] first row transition metal species should have the greatest DOS within a column, and should be best suited for chemical catalysis applications because of their anticipated rapid reactivity. Unfortunately, first row transition metal complexes are not as widely applied in catalysis even though they have two significant advantages: (1) trace contamination (e.g., drugs, food containers, etc.) is usually less of a health concern when compared to second and third row species, and (2) they are considerably less expensive.[19−21] Utilization of first row transition metal complexes is often problematic because of weaker field strengths that promote a multitude of states and $1e^-$ changes, which can be detrimental to catalysis.[22−24] Critical catalytic events typically rely on the formal shuttling of $2e^-$, such as in oxidative addition and reductive elimination.[21,24]

Carbon-based ligands can impart strong fields to a first row transition metal.[25−29] As Figure 1 illustrates, angular overlap arguments portray C-based orbitals as having very good interaction energies because of their relative proximity to appropriate metal orbitals.[18,30] In contrast, N- and O-based ligands are less well matched energetically because of their electronegativity, and overlap arguments also favor carbon ($S_C > S_N > S_O$) for related reasons, thereby contributing to the logic that carbon-based ligands are strong field in nature.

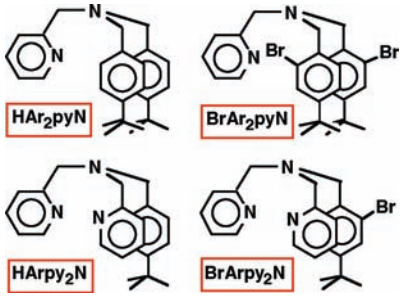

Figure 2. Initial ligand target precursors for heterolytic CH activation (HAr_2pyN and $HArpy_2N$) and oxidative addition ($BrAr_2pyN$ and $BrArpy_2N$).

Scheme 1

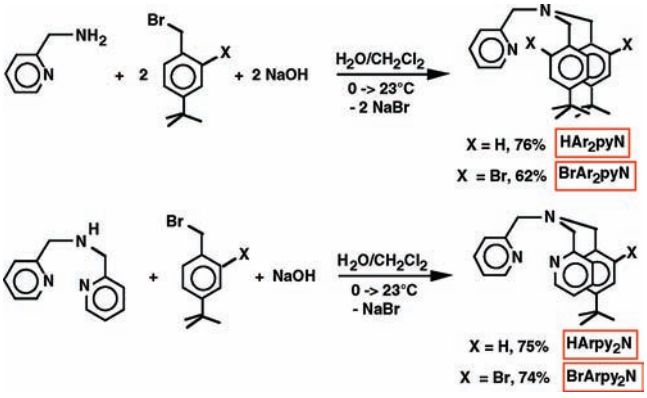

Herein are described some initial studies incorporating aryl ligands into potential tetradentate chelates to help promote stronger fields for first row transition metals. Figure 2 illustrates precursors to the ligands based on apical amine and pyridine "hooks" to enable formation of the metal-aryl bond. Two reaction types were envisioned for ligand attachment: (1) heterolytic CH-bond activation to secure metal aryl bonds from **HAr_2pyN** and **$HArpy_2N$**,[31−34] and (2) oxidative addition of aryl-Br bonds in **$BrAr_2pyN$** and **$BrArpy_2N$**.[25] Both means of attachment would lead to κ-C,C,N,N^{ax} and κ-C,N,N,N^{ax} ligation under the appropriate scenarios. During the course of these studies, the 1,3-di-2-pyridyl-2-azaallyl ligand[35] was serendipitously produced from an unusual C−N bond cleavage process, an amine debenzylation. A related degradation reported by Westerhausen led to the characterization of $(smif)_2Zn$.[36]

(18) Figgis, B. N.; Hitchman, M. A. *Ligand Field Theory and Its Applications*; Wiley-VCH: New York, 2000.
(19) de Meijere, A. *Chem. Rev.* **2000**, *100*, 2739–2740.
(20) (a) Sherry, B. D.; Furstner, A. *Acc. Chem. Res.* **2008**, *11*, 1500–1511. (2) Furstner, A.; Martin, R. *Chem. Lett.* **2005**, *34*, 624–629. (c) Furstner, A.; Leitner, A.; Mendez, M.; Krause, H. *J. Am. Chem. Soc.* **2002**, *124*, 13856–13863.
(21) Buchwald, S. L.; Bolm, C. *Angew. Chem., Int. Ed.* **2009**, *48*, 0000.
(22) (a) Klinker, E. J.; Shaik, S.; Hirao, H.; Que, L. *Angew. Chem., Int. Ed.* **2009**, *48*, 1291–1295. (b) Dhuri, S. N.; Seo, M. S.; Lee, Y. M.; Hirao, H.; Wang, Y.; Nam, W.; Shaik, S. *Angew. Chem., Int. Ed.* **2008**, *47*, 3356–3359.
(23) De Angelis, F.; Jin, N.; Car, R.; Groves, J. T. *Inorg. Chem.* **2006**, *45*, 4268–4276.
(24) For elucidation of catalysis involving $1e^-$ changes, see: Poli, R. *Angew. Chem., Int. Ed.* **2006**, *45*, 5058–5070.
(25) (a) Collman, J. P.; Hegedus, L. S.; Norton, J. R.; Finke, R. G. *Principles and Applications of Organotransition Metal Chemistry*; University Science Books: Mill Valley, CA, 1987. (b) Crabtree, R. H. *The Organometallic Chemistry of the Transition Metals*, 4th ed.; John Wiley & Sons: New York, 2005.
(26) Bower, B. K.; Tennent, H. G. *J. Am. Chem. Soc.* **1972**, *94*, 2512–2513.
(27) Byrne, E. K.; Theopold, K. H. *J. Am. Chem. Soc.* **1989**, *111*, 3887–3896.
(28) Dimitrov, V.; Linden, A. *Angew. Chem., Int. Ed.* **2003**, *42*, 2631–1633.
(29) Carnes, M.; Buccella, D.; Chen, J. Y. C.; Ramirez, A. P.; Turro, N. J.; Nuckolls, C.; Steigerwald, M. *Angew. Chem., Int. Ed.* **2009**, *48*, 290–294.
(30) Richardson, D. E. *J. Chem. Educ.* **1993**, *70*, 372.
(31) Volpe, E. C.; Chadeayne, A. R.; Wolczanski, P. T.; Lobkovsky, E. B. *J. Organomet. Chem.* **2007**, *692*, 4774–4783.
(32) (a) Hull, K. L.; Anani, W. Q.; Sanford, M. S. *J. Am. Chem. Soc.* **2006**, *128*, 7134–7135. (b) Hull, K. L.; Lanni, E. L.; Sanford, M. S. *J. Am. Chem. Soc.* **2006**, *128*, 14047–14048.
(33) Dupont, J.; Consorti, C. S.; Spencer *J. Chem. Rev.* **2005**, *105*, 2527–2571.
(34) Ryabov, A. D. *Chem. Rev* **1990**, *90*, 403–424.
(35) Frazier, B. A.; Wolczanski, P. T.; Lobkovsky, E. B.; Cundari, T. R. *J. Am. Chem. Soc.* **2009**, *131*, 3428–3429.
(36) Westerhausen, M.; Kneifel, A. N. *Inorg. Chem. Commun.* **2004**, *7*, 763–766.

Scheme 2

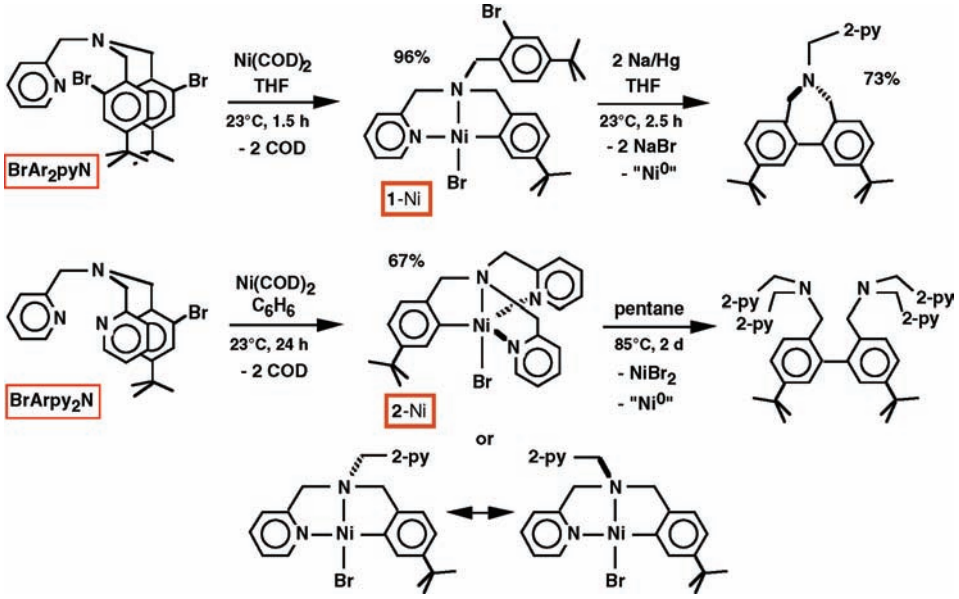

Scheme 3

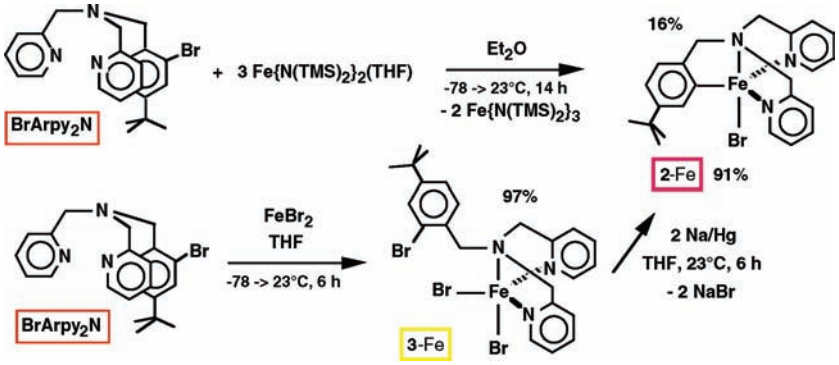

Results

Tetradentate Ligands: (2-pyridylmethyl)$_{3-x}$N(CH$_2$-Aryl)$_x$ (x = 1, 2). Scheme 1 illustrates the ligand precursor syntheses, which were essentially benzylations of 2-pyridylmethylamine and di(2-pyridylmethyl)amine. The 4-*tert*-butylbenzylbromides[37] were used to aid in the eventual solubility of the metal complexes, and the *tert*-butyl was positioned *meta* to X = H, Br to not interfere with the bond activation, yet provide some modest steric protection of the incipient metal-aryl bond. Yields were consistently around 70% for the benzylation processes, which were conducted on 4−15 g scales.

Heterolytic CH Bond Activation Attempts. Efforts to affect CH-bond activation with ligands **HAr$_2$pyN** and **HArpy$_2$N** failed despite treatment with numerous M(II) equivalents (typically halides or triflates) under a variety of conditions. Adduct formation was noted for certain halides (e.g., {κ-N,N$_{ap}$- HAr$_2$pyN}MCl$_2$; M = Fe, Co, Ni), but since subsequent CH-bond activations were not observed, even upon heating, these species were not characterized, and further synthetic efforts focused on potential oxidative addition routes.

Metalation via Oxidative Addition. 1. Nickel. In complexing first row transition metals via oxidative addition, nickel typically proves to be the easiest substrate metal because of the variety of non-carbonyl Ni(0) precursors available.[25] Metal carbonyls were avoided in the context of this study because of the potential for undesirable CO insertion into the putative M−Ar bonds. As Scheme 2 shows, treatment of Ni(COD)$_2$[38] with **BrAr$_2$pyN** afforded the orange, diamagnetic Ni(II) oxidative addition product, {κ-C,N,N^{py}-(2-pyridylmethyl)N(CH$_2$-(4-^{t}Bu-phenyl-2-yl))(CH$_2$(4-^{t}Bu-phenyl-2-Br))}NiBr (**1**-Ni) in excellent yield (96%). Attempts to connect the second aryl bond via reduction only resulted in diaryl coupling to the tertiary amine derivative shown, presumably with concomitant formation of Ni(0).

Given the history of nickel aryl−aryl couplings,[39−42] and the various oxidation states implicated,[25] the inability to affect the ultimate Ni−Ar bond formation was not

(37) Mallory, F. B.; Butler, K. E.; Berube, A.; Luzik, E. D.; Mallory, C. W.; Brondyke, E. J.; Hiremath, R.; Ngo, P.; Carroll, P. J. *Tetrahedron* **2001**, *57*, 3715–3724.

(38) Schunn, R. A. *Inorg. Synth* **1974**, *15*, 5–9.
(39) Phapale, V. B.; Cardenas, D. J. *Chem. Soc. Rev.* **2009**, *38*, 1598–1607.
(40) Denmark, S. E.; Butler, C. R. *Chem. Commun.* **2009**, 20–33.
(41) Terao, J.; Kambe, N. *Acc. Chem. Res.* **2008**, *41*, 1545–1554.
(42) Frisch, A. C.; Beller, M. *Angew. Chem., Int. Ed.* **2008**, *44*, 674–688.

surprising, hence the application of **BrArpy$_2$N** was warranted. The related treatment of Ni(COD)$_2$ with the monoarylbromide provided another orange Ni(II) oxidative addition product, {(κ-C,N,N^{py}$_2$-(2-pyridylmethyl)$_2$N(CH$_2$-(4-^{t}Bu-phenyl-2-yl))}NiBr ((Arpy$_2$N)NiBr, **2**-Ni) in 67% yield. This product manifested C_s symmetry in its ^{1}H and ^{13}C{^{1}H} NMR spectra, and is thus portrayed as a κ-C,N, N^{py}$_2$ 5-coordinate complex, although a rapid 2-pyridylmethyl exchange in the pseudo-square planar alternative cannot be ruled out. It was somewhat surprising to find that even this monoarylated complex disproportionated upon thermolysis to afford the diaryl coupling product shown. While this material may be useful as a neutral ligand framework for other, perhaps dinuclear, chelation studies, these results prompted a change away from nickel.

2. Iron. Noncarbonyl Fe(0) precursors such as "Fe(PMe$_3$)$_4$",[43] and complexes with the potential to act as Fe(0) sources such as (dmCh)$_2$Fe (dmCh = dimethylcyclohexadienyl)[44] failed to afford clean products, nor did thermolyses of Fe(II) halides, which could disproportionate to 1/3Fe(0) and 2/3Fe(III). Reasoning that solubility issues could play a major factor in disproportionation of salts or pseudo-salts, Fe{N(TMS)$_2$}$_2$(THF)[45] was chosen as a soluble Fe(II) complex capable of disproportionation. As Scheme 3 reveals, treatment of **BrArpy$_2$N** with Fe{N(TMS)$_2$}$_2$(THF) did indeed cause disproportionation to green Fe{N(TMS)$_2$}$_3$[46] and red, crystalline {κ-C,N,N^{py}$_2$-(2-pyridylmethyl)$_2$N(CH$_2$(4-^{t}Bu-phenyl-2-yl))}-FeBr ((Arpy$_2$N)FeBr, **2**-Fe). While isolated in only 16%, this is roughly 50% of the expected yield based on the disproportionation. Once characterized by X-ray crystallography, an alternative synthesis of **2**-Fe was sought. Adduct formation to give {κ-N,N^{py}$_2$-(2-pyridylmethyl)$_2$N(CH$_2$(4-^{t}Bu-phenyl-2-Br))}FeBr$_2$ (**3**-Fe) was accomplished via the combination of FeBr$_2$ and **BrArpy$_2$N** (97%), and a subsequent Na/Hg reduction afforded **2**-Br in 91% yield. A ^{1}H NMR spectrum of **2**-Fe in THF-d_8 revealed 17 different hydrogens in addition to the *tert*-butyl, indicative of plausible solvent binding.

Characterization of (Arpy$_2$N)FeBr (2-Fe). 1. X-ray Crystal Structure. Selected crystallographic data and refinement details for (Arpy$_2$N)FeBr (**2**-Fe) may be found in Table 1, and a pertinent view of the molecule is given in Figure 3. A slight twist in the aminomethylpyridine chains prevents **2**-Fe from having true C_s symmetry, but the compound is quite close to a trigonal bipyramid. The apical nitrogen and bromide span a 169.10(11)° angle about the iron, and the amine is pyramidal, with the Fe1N1C angles averaging 106.7(13)°. The bite angles of the chelate are less than 90° ($\angle$N1Fe1C15 = 80.07(17)°, $\angle$N1Fe1N2 = 75.47(15)°, $\angle$N1Fe1N3=75.19(15)°), and the corresponding Br1Fe1C15, -N2 and -N3 angles are accordingly obtuse: $\angle$Br1Fe1C15 = 110.75(14)°, $\angle$Br1Fe1N2 = 99.77(11)°, $\angle$Br1Fe1N3 = 97.86(12)°. A modest strain of chelation is transmitted to each of the equatorial ligands, as each is "tipped away" from the amine: $\angle$Fe1C15C14 = 113.0(4)°, $\angle$Fe1C15C16 = 131.8(4)°; $\angle$Fe1N2C2 = 116.5(3)°, $\angle$Fe1N2C6 = 125.3(4)°; $\angle$Fe1N3C8 = 117.6(4)°, $\angle$Fe1N3C12 = 122.5(3)°). The bond distances are all normal, with the axial amine 2.276(4) Å away from the iron in contrast to the pyridine nitrogens, which are closer at 2.149(4) and 2.156(4) Å. The iron−carbon and iron−bromide bond lengths of 2.068(5) Å and 2.5352(9) Å are typical.

2. Magnetism. The molar susceptibility and corresponding magnetic moment of (Arpy$_2$N)FeBr (**2**-Fe) are given as a function of temperature in Figure 4. The measurements are consistent with an $S = 2$ center for iron and the observed paramagnetic ^{1}H NMR spectrum, but are

Table 1. Select Crystallographic and Refinement Data for (Arpy$_2$N)FeBr (**2**-Fe) and (smif)CrN(TMS)$_2$ (**4**-Cr)

	2-Fe	**4**-Cr
formula	$C_{23}H_{26}N_3BrFe$	$C_{18}H_{28}N_4Si_2Cr$
formula wt	480.23	408.62
space group	*Pbca*	$P\bar{1}$
Z	8	2
a, Å	13.0576(12)	8.0101(4)
b, Å	16.9655(11)	11.5495(5)
c, Å	20.0495(18)	11.9921(7)
α, deg	90	95.2630(10)
β, deg	90	91.093(4)
γ, deg	90	107.584(4)
V, Å^3	4441.5(6)	1051.84(9)
ρ_{calc}, g·cm^{-3}	1.436	1.290
μ, mm^{-1}	2.491	0.666
temp, K	173(2)	173(2)
λ (Å)	0.71073	0.71073
R indices [$I > 2\sigma(I)$][a,b]	R_1 = 0.0501	R_1 = 0.0405
	wR_2 = 0.0906	wR_2 = 0.0783
R indices (all data)[a,b]	R_1 = 0.1101	R_1 = 0.0689
	wR_2 = 0.1100	wR_2 = 0.0928
GOF[c]	1.000	1.001

[a] $R_1 = \sum||F_o| - |F_c||/\sum|F_o|$. [b] $wR_2 = [\sum w(|F_o| - |F_c|)^2/\sum wF_o^2]^{1/2}$. [c] GOF (all data) = $[\sum w(|F_o| - |F_c|)^2/(n - p)]^{1/2}$, n = number of independent reflections, p = number of parameters.

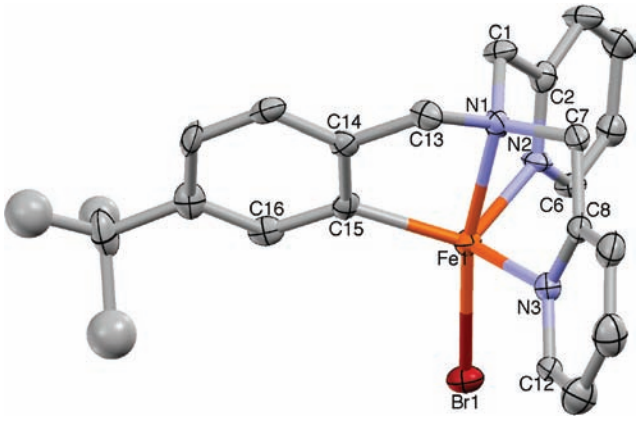

Figure 3. Molecular view of (Arpy$_2$N)FeBr (**2**-Fe); the disordered ^{t}Bu group (two staggered positions, one shown) was refined isotropically. Selected bond distances (Å) and angles (deg): Fe1N1, 2.276(4); Fe1N2, 2.149(4); Fe1N3, 2.156(4); Fe1C15, 2.068(5); Fe1Br1, 2.5352(9); N1C1, 1.461(6); N1C7, 1.466(6); N1C13, 1.467(6); N1Fe1C15, 80.07(17); N1Fe1N2, 75.47(15); N1Fe1N3, 75.19(15); N1Fe1Br1, 169.10(11); C15Fe1N2, 117.34(18); C15Fe1N3, 117.07(18); N2Fe1N3, 110.77(16); Br1Fe1C15, 110.75(14); Br1Fe1N2, 99.77(11); Br1Fe1N3, 97.86(12); Fe1C15C14, 113.0(4); Fe1C15C16, 131.8(4); Fe1N2C2, 116.5(3); Fe1N2C6, 125.3(4); Fe1N3C8, 117.6(4); Fe1N3C12, 122.5(3); Fe1N1C1, 106.7(3); Fe1N1C7, 108.0(3); Fe1N1C13, 105.5(3).

(43) Rathke, J. W.; Muetterties, E. L. *J. Am. Chem. Soc.* **1975**, *97*, 3272–3273.
(44) DiMauro, P. T.; Wolczanski, P. T. *Organometallics* **1987**, *6*, 1947–1954.
(45) (a) Olmstead, M. M.; Power, P. P.; Shoner, S. C. *Inorg. Chem.* **1991**, *30*, 2547–2551. (b) Andersen, R. A.; Faegri, K.; Green, J. C.; Haaland, A.; Lappert, M. F.; Leung, W. P.; Rypdal, K. *Inorg. Chem.* **1988**, *27*, 1782–1786.
(46) Bradley, D. C.; Copperwaithe, R. G. *Inorg. Synth* **1978**, *18*, 112–120.

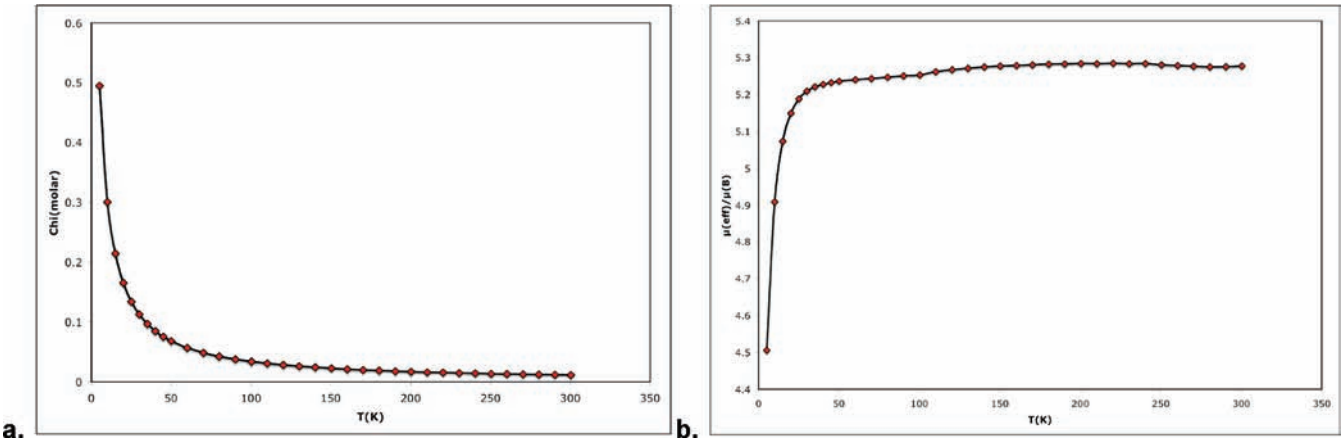

Figure 4. **a**. Molar Susceptibility (χ_M) of ($Arpy_2N$)FeBr (**2**-Fe) as a function of T(K). **b**. Magnetic moment (μ_{eff} in μ_B) of **2**-Fe as a function of T(K).

Scheme 4

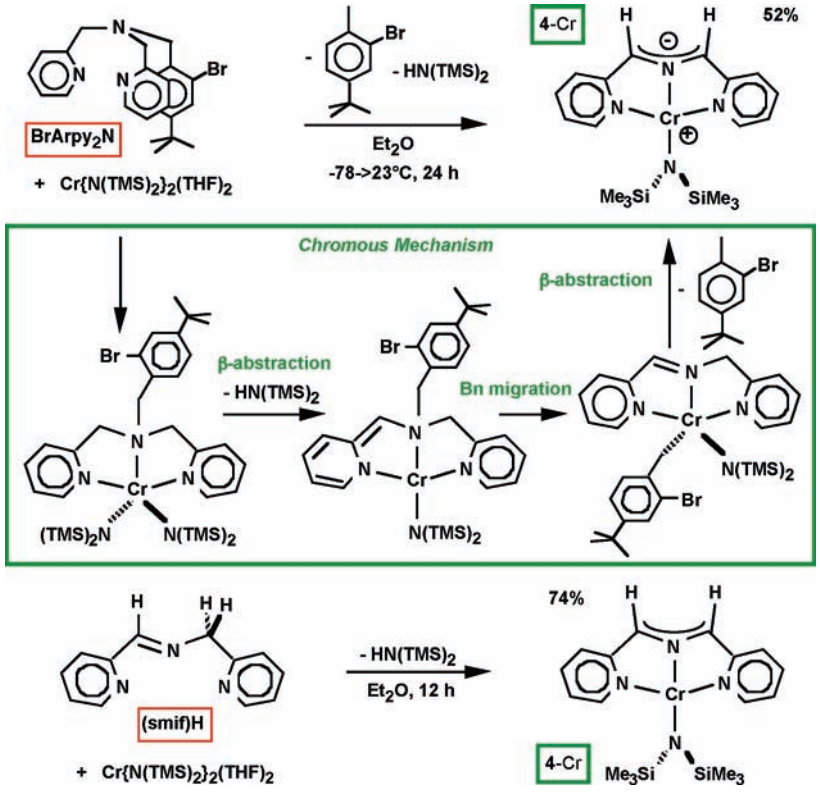

slightly high relative to the typical spin-only value of 4.90 μ_B. Unfortunately, the existence of one aryl-iron bond is not sufficient to increase the field strength enough to even achieve an intermediate spin system. The substantial decline in μ_{eff} below 50 K is attributed to the effects of zero field splitting (ZFS),[18] which can be significant in systems far afield from spherical symmetry, and the low symmetry of **2**-Fe undoubtedly contributes greatly.

C−N Bond Cleavage and Generation of (smif)CrN(TMS)$_2$ (4-Cr). In reference to the proposed disproportionation of Fe{N(TMS)$_2$}$_2$(THF)[45] to "Fe(0)" and 2 Fe{N(TMS)$_2$}$_3$,[46] the related chromium diamide, Cr{N(TMS)$_2$}$_2$(THF)$_2$,[47,48] was exposed to **BrArpy$_2$N** in diethyl ether over the course of a day at ~23 °C. Instead of the desired 5-coordinate complex, the azaallyl complex {κ-N,N^{py}$_2$-1,3-dipyridyl-2-azaallyl}CrN(TMS)$_2$ ((smif)CrN(TMS)$_2$, **4**-Cr), formed instead in >50% yield. In addition to HN(TMS)$_2$, 4-*tert*-butyl-2-bromotoluene was easily identified as a byproduct, since it is a precursor to the benzyl bromide used to prepare **BrArpy$_2$N**.[37] The reaction mixture was also unusual in the intensity of the emerald green color that increased as **4**-Cr was produced. NMR spectroscopic studies and subsequent investigations into the magnetism of **4**-Cr revealed its $S = 2$ ground state at 23 °C. Once it was identified by X-ray crystallography, an alternative route consisting of the addition

(47) Kern, R. J. *J. Inorg. Nucl. Chem* **1962**, *24*, 1105–1109.
(48) Bradley, D. C.; Hursthouse, M. B.; Newing, C. W.; Welch, A. J. *J. Chem. Soc., Chem. Commun*. **1972**, 567–568.

of 1,3-(di-2-pyridyl)-2-azapropene[49] to Cr{N(TMS)$_2$}-(THF)$_2$ was used to prepare **4**-Cr in 74% yield as shown in Scheme 4.

Characterization of (smif)CrN(TMS)$_2$ (4-Cr). 1. X-ray Crystal Structure. Selected details regarding the collection and refinement of data pertaining to (smif)CrN(TMS)$_2$ (**4**-Cr) are given in Table 1, and its molecular view can be seen in Figure 5. The complex is nearly planar, with the N-(TMS)$_2$ group essentially perpendicular to the (smif)Cr plane, but there is a slight distortion out of the plane by the amide nitrogen, with an N2Cr1N4 angle of 168.76(6)°. There is an additional asymmetry to the amide, as the Cr1N4Si2 angle of 122.23(7)° is roughly 11° greater than Cr1N4Si1 (110.97(7)°). Despite significant differences in nitrogen type, the CrN bonds of **4**-Cr are remarkably close in distance, with the pyridine nitrogens farther away from the chromium (2.0864(15), 2.0887(14) Å) than those of the azaallyl (2.0416(14) Å) and amide (2.0260(12) Å). When the entire N(TMS)$_2$ group tips relative to the (smif)Cr plane, both σ- and π-bonding effects are at play. The low symmetry allows mixing of the 4s, 4p$_x$, and 3d$_{x^2-y^2}$ orbitals with 3d$_{xz}$, thereby moderating the opposing Cr1N2 and Cr1N4 bonds. By attenuating the *trans*-influence of the opposing amide and azaallyl nitrogens via the distortion, the chromium bond distance is allowed to be shorter, thereby increasing N(pπ)-3d$_{xy}$ overlap for the half-order π-bond. This overcomes the slight loss of π-overlap due to being out of the (smif)Cr plane. Similar influences govern the cant of alkylidenes, which is often misinterpreted in the context of agostic effects.[50]

The constraints of the smif ligand[35] are revealed by the N1Cr1N3 angle of 157.07(6)°, and the cant of the pyridines that is related to that described for **2**-Fe, with outer CrNC angles of 129.3(4)° (ave) and inner CrNC angles of 112.6(6)° (ave). The bite angles of the smif ligand are 78.80(6)° (N1Cr1N2) and 78.35(6)° (N2Cr1N3), and the corresponding N$_{py}$CrN(amide) angles are 101.04(6)° and 101.74(6)°, respectively. While the strain of the bound smif is certainly evident, the bond distances suggest that the ligand imparts a relatively strong field.

2. UV−vis Spectrum. The UV−vis spectrum of (smif)-CrN(TMS)$_2$ (**4**-Cr) is shown in Figure 6, and features strong absorptions in the blue/violet and red regions of the spectrum, giving rise to the intense green transmission observed in solution. Like the previously communicated (smif)$_2$M (M = Fe, Co, Ni) and [(smif)$_2$Co]OTf complexes,[35] and (smif)$_2$M (M = V, Cr, Mn) and [(smif)$_2$Cr]-OTf compounds still undergoing investigation,[51] the spectra are likely dominated by intraligand (IL) bands, and these may be accompanied by related metal-to-ligand charge transfer bands (MLCT). The strongest feature at 396 nm ($\varepsilon \sim 27\,000$ M^{-1}cm^{-1}) is assigned to an IL transition from the azaallyl CNC^{nb} orbital to pyridine π^* orbitals.

The lower energy features at 675 nm (14,820 cm^{-1}), 627 nm (15,950 cm^{-1}), and 581 nm (17,210 cm^{-1}) are

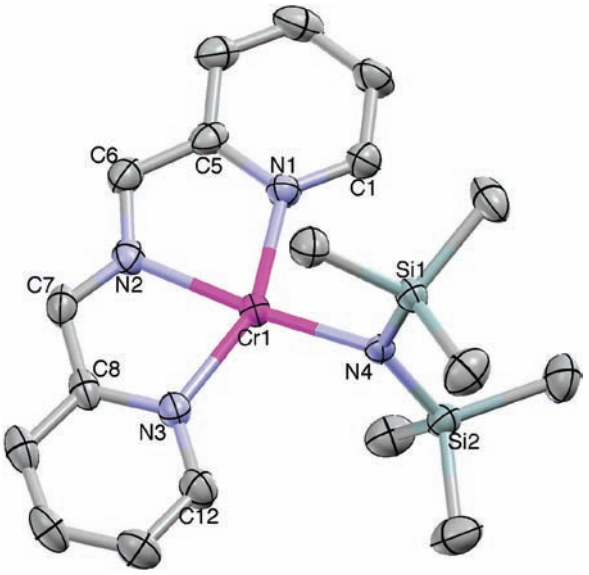

Figure 5. Molecular view of (smif)CrN(TMS)$_2$ (**4**-Cr). Selected bond distances (Å) and angles (deg): Cr1N1, 2.0887(14); Cr1N2, 2.0416(14); Cr1N3, 2.0864(15); Cr1N4, 2.0260(12); N2C6, 1.332(2); N2C7, 1.320(2); N4Si1, 1.6967(14); N4Si2, 1.6913(14); N1Cr1N3, 157.07(6); N2Cr1N4, 168.76(6); N1Cr1N2, 78.80(6); N1Cr1N4, 101.04(6); N2Cr1N3, 78.35(6); N3Cr1N4, 101.74(6); Cr1N1C1, 129.05(12); Cr1N1C5, 112.12(12); Cr1N3C12, 129.57(13); Cr1N3C8, 113.02(12); Cr1N2C6, 115.65(13); Cr1N2C7, 115.77(13); C6N2C7, 128.48(17); Cr1N4Si1, 110.97(7); Cr1N4Si2, 122.23(7).

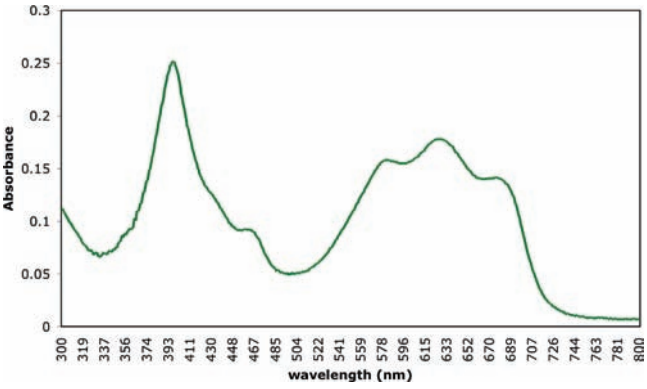

Figure 6. UV−vis spectrum of (smif)CrN(TMS)$_2$ (**4**-Cr): 396 nm ($\varepsilon \sim 27\,000$ M^{-1} cm^{-1}), 424 (sh, $\varepsilon \sim 12\,500$ M^{-1} cm^{-1}), 461 nm ($\varepsilon \sim 9\,500$ M^{-1} cm^{-1}), 581 nm ($\varepsilon \sim 17\,000$ M^{-1} cm^{-1}), 627 nm ($\varepsilon \sim 19\,000$ M^{-1} cm^{-1}), 675 nm ($\varepsilon \sim 15\,000$ M^{-1} cm^{-1}).

difficult to assess, but are in the region expected for the lower energy IL band, which is also CNC^{nb}→py-π^*. Calculations on related complexes (e.g., (smif)$_2$Cr)[51] suggest that the CNC^{nb} orbital is energetically near the lower lying 3d orbitals of the square plane; hence it is possible that some of the bands may be MLCT in character. However, related features have been observed in several complexes containing the rigid CNC backbone, and the separations between the bands of roughly 1130 and 1260 cm^{-1} suggests that they may be vibronic components of a single electronic absorption. The fact that the separations between absorption maxima are slightly different would be expected if other, weaker absorptions, such as MLCT and d-d bands, were underlying, thereby skewing the progression. The IR spectrum of **4**-Cr manifests a sharp absorption at 1140 cm^{-1}, which likely corresponds to a

(49) Incarvito, C.; Lam, M.; Rhatigan, B.; Rheingold, A. L.; Qin, C. J.; Gavrilova, A. L.; Bosnich, B. *J. Chem. Soc., Dalton Trans.* **2001**, 3478–3488.
(50) Goddard, R. J.; Hoffmann, R.; Jemmis, E. D. *J. Am. Chem. Soc.* **1980**, *102*, 7667–7676.
(51) Frazier, B. A.; Lobkovsky, E. B.; Wolczanski, P. T.; Doucette, S.; Mossin, S.; Meyer, K.; DeBeer George, S.; Cundari, T. R.; Hachmann, J.; Chan, G. K.-L., manuscript in preparation.

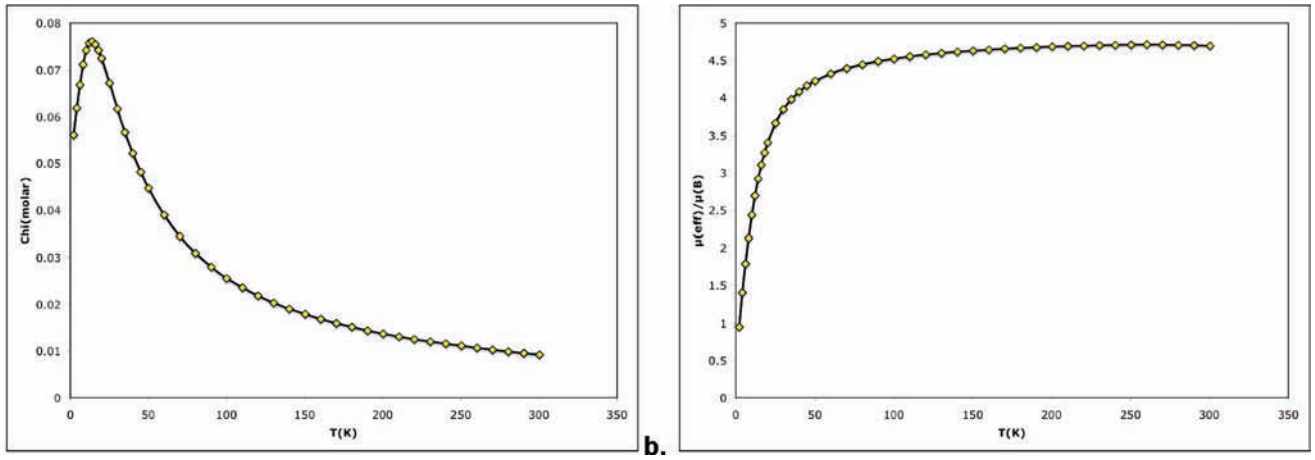

Figure 7. **a.** Molar Susceptibility (χ_M) of (smif)CrN(TMS)$_2$ (**4**-Cr) as a function of T(K). **b.** Magnetic moment (μ_{eff} in μ_B) of **4**-Cr as a function of T(K).

CNC bending vibration that has the appropriate symmetry to couple with the electronic IL transition. It is not uncommon for IL bands to show vibrational components in solution at room temperature.[52,53]

3. Magnetism. Magnetic susceptibility measurements on (smif)CrN(TMS)$_2$ (**4**-Cr) show a μ_{eff} of ~4.7 μx_B at 23 °C that is fully consistent with the expected $S = 2$ chromium(II) center (Figure 7). Note that the susceptibility is strongly attenuated below 50 K. While it is conceivable that strong intermolecular interactions may be present, the more likely explanation for the dramatic downturn in χ_M and μ_{eff} below 50 K is the effect of the extremely low symmetry in the system coupled with spin−orbit coupling, that is, zero field splitting (ZFS). While it may not be common to find ZFS effects so pronounced, it is prudent to recognize that the gross deviation from spherical symmetry that characterizes this system is exactly the instance in which low symmetry effects are maximized. It is interesting to compare **4**-Cr with (Arpy$_2$N)FeBr (**2**-Fe, Figure 4); both $S = 2$ systems show significant ZFS, but the onset of the downturn occurs at a much higher temperature for the lower symmetry, pseudo-square planar derivative.

Discussion

Aryl-Containing Chelates. The concept of using aryl-based chelates to impart strong fields to first row transition metal complexes has not been realized by the examples above, which are ambiguous at best in addressing this issue. While $S = 0$ derivatives of square planar (and possibly tbp) Ni(II) were prepared, high spin species are typically found only for truly weak field ligands, or in specific steric situations; hence their diamagnetism is not enough to fully support the contention of significantly greater fields. (Arpy$_2$N)FeBr (**2**-Fe) was characterized as an $S = 2$ species, thus the monoarylated ligand framework failed to even produce an intermediate spin (i.e., $S = 1$) system that might be expected for a stronger field ligand. Clearly, these results suggest that more than one metal-aryl bond will be necessary to generate the fields equated with low spin complexes.

Serendipitous (smif)CrN(TMS)$_2$ Formation. The most interesting discovery in this work concerns the serendipitous formation of the 1,3-di-2-pyridyl-2-azaallyl or "smif" complex (smif)CrN(TMS)$_2$ (**4**-Cr), whose relatively clean formation from Cr{N(TMS)$_2$}$_2$(THF)$_2$ and **BrArpy$_2$N** remains mysterious. In Scheme 4, a mechanism is shown that avoids redox changes that are expected to be deleterious to the ultimate generation of a chromous product. It is expected that any Cr(III) intermediate(s) would be difficult to reduce back to Cr(II), and the oxidation to Cr(IV) by an aryl-halide has only modest precedent; hence a process that holds the chromous oxidation state constant has considerable merit.[54−57] In the proposed process shown, adduct formation to give (κ-N,N$^{py}_2$-BrArpy$_2$N)Cr{N(TMS)$_2$}$_2$ is followed by a β-abstraction[58] of a methylene hydrogen adjacent to the amine by a basic N(TMS)$_2$ group, rendering the smif precursor monoanionic. A simple elimination of 4-*tert*-butyl-2-Br-toluene from the ligand backbone would directly generate **4**-Cr, but it is difficult to conceive of how the chromium could facilitate this process, which is basically not a standard organic reaction. Instead, an α-migration of the benzyl group is proposed,[25] thereby returning the chelate to neutrality as (smif)H, that is, the bound 1,3-(di-2-pyridyl)-2-azapropene, yet keeping the chromium in its +2 oxidation state. A second β-abstraction of the remaining methylene hydrogen—this time by the benzyl—generates **4**-Cr via the release of 4-*tert*-butyl-2-Br-toluene. A similar sequence can be envisaged for Westerhausen's preparation of (smif)$_2$Zn from ZnMe$_2$ and (2-pyridylmethyl)$_2$NH;[36] it is certainly likely that no redox changes occur in the zinc reaction.

NHC Analogue: smif. From the X-ray crystal structure of (smif)CrN(TMS)$_2$ (**4**-Cr), it can be inferred that the

(52) (a) Mack, J.; Stillman, M. J.; Kobayashi, N. *Coord. Chem. Rev.* **2007**, *251*, 429–453. (b) Mack, J.; Stillman, M. J. *Coord. Chem. Rev.* **2001**, *219−221*, 993–1032.
(53) (a) Güdel, H. U.; Zilian, A. *Coord. Chem. Rev.* **1991**, *111*, 33–38. (b) Colombo, M. G.; Brunold, T. C.; Riedener, T.; Güdel, H. U.; Förtsch, M.; Bürgi, H.-B. *Inorg. Chem.* **1994**, *33*, 545–550.
(54) Okazoe, T.; Takai, K.; Utimoto, K. *J. Am. Chem. Soc.* **1987**, *109*, 951–953.
(55) Wessjohann, L. A.; Schmidt, G.; Schrekker, H. S. *Tetrahedron* **2008**, *64*, 2134–2142.
(56) Shinokubo, H.; Oshima, K. *Eur. J. Org. Chem.* **2004**, 2081–2091.
(57) Takai, K.; Nozaki, H. *Proc. Jpn. Acad., Ser. B* **2000**, *76*, 123–131.
(58) Hirsekorn, K. F.; Veige, A. S.; Marshak, M. P.; Koldobskaya, Y.; Wolczanski, P. T.; Cundari, T. R.; Lobkovsky, E. B. *J. Am. Chem. Soc.* **2005**, *127*, 4809–4830.

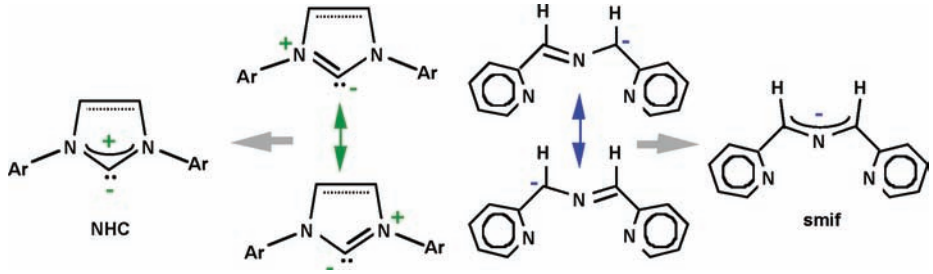

Figure 8. Lewis structures for *N*-heterocyclic carbenes (NHC) and smif showing isoelectronic features.

azaallyl backbone of the smif ligand possesses a relatively strong field character, as its CrN bond, whose distance is 2.0416(14) Å, effectively competes with the *trans*-amide interaction (2.0258(13) Å). While the pyridine portions of the chelate undoubtedly help keep the azaallyl interaction close, the charged nature of the ligand must provide an ionic contribution to the bond that renders it stronger than a typical pyridine or imine. Figure 8 illustrates the relationship between smif and N-heterocyclic carbenes (NHC), which are generally considered strong field ligands.[59,60] The NHC ligands contain a neutral NCN linkage that is isoelectronic to the anionic CNC^- backbone of smif. While the N-donor smif presumably has lesser overlap and a greater ΔE (Figure 1) relative to the NHC's carbon-donor, it is reasonable to assume that the charge helps compensate.

Conclusions

One aryl-metal bond imbedded into a chelate system otherwise composed of metal−nitrogen bonds does not appear to be enough to engender strong fields about first row transition elements. The elaboration of multiple M−Ar bonds into chelates is ongoing. The azaally backed ligand smif shows considerable promise as a moderate field strength ligand capable of supporting low symmetry complexes with unusual optical properties.

Experimental Section

General Considerations. All manipulations were performed using either glovebox or high vacuum line techniques. Hydrocarbon solvents containing 1−2 mL of added tetraglyme, and ethereal solvents were distilled under nitrogen from purple sodium benzophenone ketyl and vacuum transferred from same prior to use. Benzene-d_6 and toluene-d_8 were dried over sodium, vacuum transferred and stored under N_2. THF-d_8 was dried over sodium benzophenone ketyl. Methylene chloride-d_2 was dried over CaH_2, vacuum transferred and stored over activated 4 Å molecular sieves. $Ni(COD)_2$,[38] $CrCl_2(THF)$,[47] Fe{$N(TMS)_2$}$_2$(THF),[45] 2-bromo-4-*tert*-butylbenzyl bromide,[37] and 1,3-(2-pyridyl)-2-azapropene ((smif)H)[49] were prepared according to literature procedures. All other chemicals were commercially available and used as received. All glassware was oven-dried.

NMR spectra were obtained using Varian XL-400, INOVA 400, and Unity-500 spectrometers. Chemical shifts are reported relative to benzene-d_6 (^{1}H δ 7.16; ^{13}C{^{1}H} δ 128.39), toluene-d_8 (^{1}H δ 2.09; ^{13}C{^{1}H} δ 20.4), thf-d_8 (^{1}H δ 3.58; ^{13}C{^{1}H} δ 67.57), and methylene chloride-d_2 (^{1}H δ 5.32; ^{13}C{^{1}H} δ 54.00). Infrared spectra were recorded on a Nicolet Avatar 370 DTGX spectrophotometer interfaced to an IBM PC (OMNIC software). UV−vis spectra were obtained on a Shimadzu UV-2102 interfaced to an IBM PC (UV Probe software). GC-MS spectra were obtained on a JEOL GCMate 2 mass spectrometer coupled to an Agilent 689 N GC with EI ionization under standard conditions. Solution magnetic measurements were conducted via Evans' method in toluene-d_8.[61] Solid state magnetic measurements were performed using a Johnson Matthey magnetic susceptibility balance calibrated with $HgCo(SCN)_4$. Elemental analyses were performed by Robertson Microlit Laboratories, Madison, NJ, and by services at the University of Erlangen-Nuremberg, Germany.

Procedures. 1. *N*,*N*-bis(4-*tert*-butylbenzyl)-1-(pyridine-2-yl)-methanamine. (HAr$_2$pyN). To a 0 °C biphasic solution of 2-(aminomethyl)pyridine (1.500 g, 13.87 mmol) in 10 mL of H_2O and 4-*tert*-butylbenzyl bromide (6.302 g, 27.74 mmol) in 70 mL of CH_2Cl_2 was slowly added a solution of NaOH (1.110 g, 27.75 mmol) in 10 mL of H_2O. The biphasic reaction mixture was slowly warmed to 23 °C, while stirring vigorously, and monitored by pH. When the reaction mixture was neutral, the product was extracted from the aqueous layer with CH_2Cl_2 (4 × 15 mL). Organic layers were combined, dried over $MgSO_4$, and filtered. Rotary evaporation of the filtrate yielded a red-orange oil. After the addition of hexanes, a brown impurity was filtered. The hexanes filtrate was concentrated, cooled, and yielded yellow crystals of **HAr$_2$pyN**. (4.198 g, 76%). ^{1}H NMR (C_6D_6, 400 MHz): δ 1.25 (s, C(CH_3)$_3$,18 H), 3.64 (s, CH_2, 4 H), 3.93 (s, CH_2, 2 H), 6.63 (t, py-C^4*H*,1 H, J = 4.8 Hz), 7.14 (t, py-C^5*H*, 1 H, J = 4.8 Hz), 7.31 (d, C^{2,6}*H*, 4 H, J = 8 Hz), 7.43 (d, C^{3,5}*H*, 4 H, J = 8 Hz), 7.55 (d, py-C^3*H*, 1 H, J = 8 Hz), 8.48 (d, py-C^6*H*, 1 H, J = 5 Hz).^{13}C{^{1}H} NMR (C_6D_6, 100 MHz): δ 31.89 (C(CH_3)$_3$), 34.81 (*C*(CH_3)$_3$), 58.41 (*C*H_2), 60.21 (*C*H_2), 122.05 (py-*C*^{5}H), 122.97 (py-*C*^{3}H), 125.82 (*C*^{3}H), 129.19 (*C*^{2}H), 136.22 (py-*C*^{4}H), 137.24 (*C*^{1}H), 149.62 (py-*C*^{6}H), 150.07 (*C*^{4}H), 161.29 (py-*C*^{2}H).

2. *N*-(4-*tert*-butylbenzyl)-1-(pyridine-2-yl)-*N*-(pyridine-2-yl-methyl)methanamine (HArpy$_2$N). To a 0 °C biphasic solution of 2-dipicolylamine (5.000 g, 25.10 mmol) in 100 mL of CH_2Cl_2 and 4-*tert*-butylbenzyl bromide (5.700 g, 25.10 mmol) in 40 mL of H_2O was slowly added a solution of NaOH (1.004 g, 25.10 mmol) in 10 mL of H_2O. The canary yellow biphasic reaction mixture was slowly warmed to 23 °C, while stirring vigorously, and monitored by pH. When the reaction mixture was neutral, the product was extracted from the aqueous layer with CH_2Cl_2 (4 × 15 mL). Organic layers were combined, dried over $MgSO_4$, and filtered. Rotary evaporation of the filtrate yielded an orange-yellow oil. After the addition of hexanes, a brown impurity was filtered. The hexanes filtrate was concentrated, cooled, and yielded yellow crystals of **HArpy$_2$N** (6.499 g, 75%). ^{1}H NMR (C_6D_6, 400 MHz): δ 1.23 (s, C(CH_3)$_3$, 9 H), 3.69 (s, CH_2, 2 H), 3.97 (s, CH_2, 4 H), 6.63 (t, py-C^4*H*, 2 H, J = 5.6 Hz), 7.13 (t, py-C^5*H*, 2 H, J = 7.6 Hz), 7.29 (d, C^{2,6}*H*, 2 H, J = 8 Hz), 7.42 (d, C^{3,5}*H*, 2 H, J = 8 Hz), 7.50 (d, py-C^3*H*, 2 H, J = 7.9 Hz),

(59) Jacobsen, H.; Correa, A.; Poater, A.; Costabile, C.; Cavallo, L. *Coord. Chem. Rev.* **2009**, *253*, 687–703.
(60) de Fremont, P.; Marion, N.; Nolan, S. P. *Coord. Chem. Rev.* **2009**, *253*, 862–892.
(61) (a) Evans, D. F. *J. Chem. Soc.* **1959**, 2003–2005. (b) Schubert, E. M. *J. Chem. Educ.* **1992**, *69*, 62.

8.48 (d, py-C^6*H*, 2 H, J = 4.6 Hz). ^{13}C{^{1}H} NMR (C_6D_6, 100 MHz) δ: 31.86 (C(*C*H$_3$)$_3$), 34.80 (*C*(CH$_3$)$_3$), 58.56 (*C*H$_2$), 60.48 (*C*H$_2$), 122.10 (py-*C*^{5}H), 123.11 (py-*C*^{3}H), 125.81 (*C*^{3}H), 129.27 (*C*^{2}H), 136.21 (py-*C*^{4}H), 137.06 (*C*^{1}H), 149.75 (py-*C*^{6}H), 150.09 (*C*^{4}H), 160.91 (py-*C*^{2}H).

3. *N*,*N*-bis(2-bromo-4-*tert*-butylbenzyl)-1-(pyridine-2-yl)methanamine (BrAr$_2$pyN). To a 0 °C biphasic solution of 2-(aminomethyl)pyridine (1.000 g, 9.25 mmol) in 10 mL of H_2O and 2-bromo-4-*tert*-butylbenzyl bromide (5.660 g, 18.50 mmol) in 60 mL of CH_2Cl_2 was slowly added a solution of NaOH (0.740 g, 18.50 mmol) in 10 mL of H_2O. The biphasic reaction mixture was slowly warmed to 23 °C, while stirring vigorously, and turned red within 2 h. The organic layer became orange upon complete conversion to product. The product was extracted from the aqueous layer with CH_2Cl_2 (3 × 15 mL). Organic layers were combined, dried over Na_2SO_4, and filtered. Rotary evaporation of the filtrate yielded an orange oil. After the addition of hexanes, a brown impurity was filtered. The hexanes filtrate was concentrated and cooled to form orange-yellow crystals of **BrAr$_2$pyN** (16.16 g, 62%). ^{1}H NMR (C_6D_6, 400 MHz): δ 1.06 (s, C(C*H*$_3$)$_3$, 18 H), 3.96 (s, C*H*$_2$, 6 H), 6.59 (t, py-C^4*H*, 1 H, J = 5.8 Hz), 7.06 (t, py-C^5*H*, 1 H, J = 7.6 Hz), 7.10 (d, C^4*H*, 2H, J = 8 Hz), 7.33 (d, py-C^3*H*, 1 H, J = 8 Hz), 7.62 (s, C^6*H*, 2 H), 7.76 (d, C^3*H*, 2 H, J = 8 Hz), 8.48 (d, py-C^6*H*, 1 H, J = 5.6 Hz). ^{13}C{^{1}H} NMR (C_6D_6, 100 MHz) 31.46 (C(*C*H$_3$)$_3$), 34.73 (*C*(CH$_3$)$_3$), 58.53 (*C*H$_2$), 60.60 (*C*H$_2$), 122.17 (py-*C*^{5}H), 123.19 (py-*C*^{3}H), 125.08 (*C*^{1}H), 125.15 (*C*^{4}H), 130.43 (*C*^{6}H), 130.78 (*C*^{3}H), 136.18 (py-*C*^{4}H), 136.35 (*C*^{2}H), 149.86 (py-*C*^{6}H), 152.23 (*C*^{5}H), 160.26 (py-*C*^{2}H). MS: *m*/*z* (%) 464, 466, 468 (58), 331, 333 (36), 225, 227 (50), 93 (100), M$^+$ not observed.

4. *N*-(2-bromo-4-*tert*-butylbenzyl)-1-(pyridine-2-yl)-*N*-(pyridine-2-ylmethyl)methanamine. (BrArpy$_2$N). To a 0 °C biphasic solution of 2-dipicolylamine (10.000 g, 50.19 mmol) in 100 mL of CH_2Cl_2 and 2-bromo-4-*tert*-butylbenzylbromide (15.36 g, 50.19 mmol) in 50 mL of H_2O was slowly added a solution of NaOH (2.01 g, 50.3 mmol) in 20 mL of H_2O. The orange biphasic reaction mixture was slowly warmed to 23 °C, while stirring vigorously, and monitored by pH. When the mixture was neutral, the product was extracted from the aqueous layer with CH_2Cl_2. Organic layers were combined, dried over $MgSO_4$, and filtered. Rotary evaporation of the filtrate yielded a tan-yellow solid. After hot filtration of the solid in hexanes, tan-yellow crystals were isolated from the filtrate a **BrArpy$_2$N** (15.713 g, 74%). ^{1}H NMR (C_6D_6, 400 MHz): δ 1.06 (s, C(C*H*$_3$)$_3$, 9 H), 3.98 (s, C*H*$_2$, 6 H), 6.60 (t, py-C^4*H*, 2 H, J = 8 Hz), 7.10 (t, py-C^5*H*, C^4*H*, 3 H, J = 8 Hz), 7.45 (d, py-C^3*H*, 2 H, J = 7.8 Hz), 7.63 (s, C^6*H*, 1 H), 7.78 (d, C^3*H*, 1 H, J = 8 Hz), 8.47 (d, py-C^6*H*, 2 H, J = 4.6 Hz). ^{13}C{^{1}H} NMR (C_6D_6, 100 MHz): δ 31.47 (C(*C*H$_3$)$_3$), 34.73 (*C*(CH$_3$)$_3$), 58.62 (*C*H$_2$), 60.52 (*C*H$_2$), 122.16 (py-*C*^{5}H), 123.37 (py-*C*^{3}H), 125.07 (*C*^{1}H), 125.25 (*C*^{4}H), 130.43 (*C*^{6}H), 131.18 (*C*^{3}H), 136.20 (py-*C*^{4}H), 136.50 (*C*^{2}H), 149.79 (py-*C*^{6}H), 152.21 (*C*^{5}H), 160.43 (py-*C*^{2}H).

5. {κ-C,N,N^{py}-(2-pyridylmethyl)N(CH$_2$(4-^{t}Bu-phenyl-2-yl))-(CH$_2$(4-^{t}Bu-phenyl-2-Br))}NiBr (1-Ni). To a 100 mL flask charged with Ni(COD)$_2$ (1.000 g, 3.64 mmol) and **BrAr$_2$pyN** (2.03 g, 3.64 mmol) was vacuum transferred 60 mL of THF at −78 °C. After slowly warming to 23 °C, the reaction mixture was stirred for 1 h and filtered. The filtrate was concentrated, cooled to −78 °C, and filtered to yield 2.15 g **1**-Ni as a crystalline orange solid (96%). ^{1}H NMR (C_6D_6, 400 MHz): δ 0.88 (s, C(C*H*$_3$)$_3$, 9 H), 1.47 (s, C(C*H*$_3$)$_3$, 9 H), 3.38 (d, C*H*$_2$, 1 H, J = 14.4 Hz), 3.43 (d, C*H*$_2$, 1 H, J = 16 Hz), 3.49 (d, C*H*$_2$, 1 H, J = 13.2 Hz), 4.15 (d, C*H*$_2$, 2 H, J = 13.2 Hz), 5.18 (d, C*H*$_2$, 1 H, J = 14 Hz), 6.03 (t, py-C^4*H*, 1 H, J = 6 Hz), 6.23 (d, 1 H, J = 7.6 Hz), 6.49 (t, py-C^5*H*, 1 H, J = 7.6 Hz), 6.69 (d, C^4*H*, 1 H, J = 7.6 Hz), 6.97 (s, C^6*H*, 1 H), 7.04 (t, C^{3,4}*H*, 2 H, J = 7.6 Hz), 8.58 (s, C^6*H*, 1 H), 8.82 (d, py-C^6*H*, 1 H, J = 4.8 Hz), 10.13 (d, C^3*H*, 1 H, J = 8 Hz). ^{13}C{^{1}H} NMR (C_6D_6, 100 MHz): δ 31.04 (C(*C*H$_3$)$_3$), 32.40 (C(*C*H$_3$)$_3$), 34.72 (*C*(CH$_3$)$_3$), 35.40 (*C*(CH$_3$)$_3$), 63.67 (*C*H$_2$), 64.93 (*C*H$_2$), 70.92 (*C*H$_2$), 119.45 (*C*^{6}H), 120.95 (*C*^{1}H), 121.90 (py-*C*^{5}H), 122.33 (py-*C*^{3}H), 125.35 (*C*^{6}H), 125.99 (*C*^{4}H), 129.20 (*C*^{3}H), 131.46 (*C*^{3}H), 136.12 (*C*^{4}H), 136.59 (*C*^{2}H), 140.30 (py-*C*^{4}H), 141.96 (*C*^{2}H), 147.91(*C*^{5}H), 148.71(*C*^{5}H), 150.42 (py-*C*^{6}H), 153.84 (py-*C*^{2}H), 160.90 (*C*^{1}H). Anal. Calcd $H_{28}C_{34}N_2Br_2Ni$: C, 54.50; H, 5.55; N, 4.54. Found: C, 54.65, 54.71; H, 5.64, 5.64; N, 4.03, 4.07.

6. 2,10-Di-*tert*-butyl-6-(pyridine-2-ylmethyl)-6,7-dihydro-5*H*-dibenzo[*c*,*e*]azepine (Coupled BrAr$_2$pyN). To a 50 mL round-bottom flask charged with **1**-Ni (0.350 g, 0.57 mmol) and 0.95% sodium amalgam (0.026 g Na, 1.13 mmol) was vacuum transferred 25 mL of THF at −78 °C. Upon warming to 23 °C and stirring for 30 min, the orange reaction mixture turned orange-brown. After stirring at 23 °C for 7 h, volatiles were removed in vacuo leaving a brown solid (0.164 g, 73%). ^{1}H NMR (C_6D_6, 400 MHz): δ 1.30 (s, C(C*H*$_3$)$_3$, 18 H), 3.51 (s, C*H*$_2$, 4 H), 3.98 (s, C*H*$_2$, 2 H), 6.71 (t, py-C^4*H*, 1 H, J = 5.5 Hz), 7.19 (t, py-C^5*H*, 1 H, J = 7.3 Hz), 7.30 (s, C^{5,6}*H*, 4 H), 7.60 (d, py-C^3*H*, 1 H, J = 7.8 Hz), 7.71 (s, C^3*H*, 2 H), 8.57 (d, py-C^6*H*, 1 H, J = 4 Hz). ^{13}C{^{1}H} NMR (C_6D_6, 125 MHz): δ 31.03 (C(*C*H$_3$)$_3$), 35.07 (*C*(CH$_3$)$_3$), 55.55 (*C*H$_2$), 61.85 (*C*H$_2$), 122.22 (py-*C*^{5}H), 123.65 (py-*C*^{3}H), 125.16 (*C*^{5}H), 125.28 (*C*^{3}H), 130.55 (*C*^{6}H), 133.21 (*C*^{1}H), 136.41 (py-*C*^{4}H), 142.32 (*C*^{2}H), 149.75 (py-*C*^{6}H), 151.27 (*C*^{4}H), 161.30 (py-*C*^{2}H). MS: *m*/*z* (%) 306 (100), 93 (30), 57 (15), M$^+$ not observed.

7. {κ-C,N,N$^{py}_2$-(2-pyridylmethyl)$_2$N(CH$_2$(4-^{t}Bu-phenyl-2-yl))}NiBr (2-Ni). To a 100 mL round-bottom flask charged with Ni(COD)$_2$ (0.324 g, 1.18 mmol) and **BrArpy$_2$N** (0.500 g, 1.18 mmol) was vacuum transferred 50 mL of benzene. The red-orange reaction mixture was stirred at 23 °C for 24 h while orange needles precipitated from solution. The reaction was filtered to yield microcrystalline orange needles of **2**-Ni (0.380 g, 67%). ^{1}H NMR (THF-d$_8$, 400 MHz): δ 1.27 (s, C(C*H*$_3$)$_3$, 9 H), 4.39 (d, C*H*$_2$, 2 H, J = 13.8 Hz), 4.45 (s, C*H*$_2$, 2 H), 4.87 (d, C*H*$_2$, 2 H, J = 13.9 Hz), 6.76 (d, C^4*H*, 1 H, J = 7.7 Hz), 6.82 (d, C^3*H*, 1 H, J = 7.3 Hz), 7.07 (t, py-C^4*H*, 2 H, J = 6.6 Hz), 7.63 (t, py-C^5*H*, 2 H, J = 7.8 Hz), 7.86 (d, py-C^3*H*, 2 H, J = 7.5 Hz), 8.34 (s, C^6*H*, 1 H), 8.57 (d, py-C^6*H*, 2 H, J = 4.7 Hz). ^{13}C{^{1}H} NMR (THF-d$_8$, 100 MHz) δ: 32.34 (C(*C*H$_3$)$_3$), 64.17 (*C*H$_2$), 69.75 (*C*H$_2$), 121.34 (*C*^{3}H), 122.16 (py-*C*^{5}H), 124.02 (py-*C*^{3}H), 125.26 (*C*^{5}H), 138.01 (py-*C*^{4}H), 141.01(*C*^{4}H), 150.40 (py-*C*^{6}H), 158.63 (*C*^{1}H). Anal. Calcd $H_{26}C_{23}N_3BrNi$: C, 57.19; H, 5.42; N, 8.70. Found: C, 56.43, 56.26; H, 5.26, 5.20; N, 8.45, 8.33.

8. *N*,*N*′-(5,5′-di-*tert*-butylbiphenyl-2,2′-diyl)bis(methylene)bis-(1-pyridin-2-yl)-*N*-(pyridine-2-ylmethyl)methanamine) (Coupled BrArpy$_2$N). Thermolysis of **2**-Ni in pentane at 85 °C for 2 d led to the formation of coupled ligand, and, presumably NiBr$_2$ and Ni^0. ^{1}H NMR (C_6D_6, 400 MHz): δ 1.22 (s, C(C*H*$_3$)$_3$, 9 H), 3.70 (s, C*H*$_2$, 2 H), 3.97 (s, C*H*$_2$, 2 H), 6.62 (t, py-C^4*H*, 2 H, J = 5.8 Hz), 7.11 (t, py-C^5*H*, 2 H, J = 7.3 Hz), 7.36 (s, C^3*H*, 1 H), 7.43 (d, C^{5,6}*H*, 2 H, J = 8.1 Hz), 7.51 (d, py-C^3*H*, 2 H, J = 7.7 Hz), 8.52 (d, py-C^6*H*, 2 H, J = 4 Hz). ^{13}C{^{1}H} NMR (C_6D_6, 125 MHz): δ 31.87 (C(*C*H$_3$)$_3$), 35.00 (*C*(CH$_3$)$_3$), 58.54 (*C*H$_2$), 60.44 (*C*H$_2$), 122.07 (py-*C*^{5}H), 122.15 (py-*C*^{3}H), 123.29 (*C*^{5}H), 124.76 (*C*^{3}H), 125.80 (*C*^{6}H), 136.23 (py-*C*^{4}H), 137.18 (*C*^{1}H), 149.69 (*C*^{2}H), 149.76 (py-*C*^{6}H), 149.90 (*C*^{4}H), 157.93 (py-*C*^{2}H).

9. {κ-C,N,N$^{py}_2$-(2-pyridylmethyl)$_2$N(CH$_2$(4-^{t}Bu-phenyl-2-yl))}FeBr (2-Fe). a. To a 25 mL round-bottom flask charged with Fe{N(SiMe$_3$)$_2$}$_2$(THF) (0.250 g, 0.56 mmol) and **BrArpy$_2$N** (0.473 g, 1.11 mmol) was vacuum transferred 10 mL of Et$_2$O at −78 °C. The dark green reaction mixture was slowly warmed to 23 °C. The reaction stirred for 14 h prior to removing all volatiles and triturating with pentane. The green solid was taken up in benzene and filtered through a Celite plug. Red, rod-shaped crystals of **2**-Fe were obtained in 16% yield (0.043 g). **b.** To a 100 mL round-bottom flask containing **3**-Fe (0.900 g, 1.41 mmol) and 0.95% sodium amalgam (0.066 g, 2.88 mmol Na) was vacuum transferred 50 mL of THF at −78 °C. The reaction mixture became red after it was stirred at 23 °C for 2 h. Volatiles

were removed in vacuo yielding an orange-red solid. The solid was dissolved in THF and filtered through Celite. The filtrates were concentrated to yield **2**-Fe as an orange powder (0.617 g, 91%). ^{1}H NMR (THF-d_8, 400 MHz): δ −37.15 ($\upsilon_{1/2} \approx 26$ Hz, 1 H), −11.47 ($\upsilon_{1/2} \approx 29$ Hz, 1 H), 0.45 ($\upsilon_{1/2} \approx 15$ Hz, 1 H), 5.75 ($\upsilon_{1/2} \approx\approx 49$ Hz, 1 H), 6.35 ($\upsilon_{1/2} \approx 40$ Hz, 1 H), 10.96 ($\upsilon_{1/2} \approx 22$ Hz, C(C*H*$_3$)$_3$, 9 H), 33.52 ($\upsilon_{1/2} \approx 462$ Hz, 1 H), 41.68 ($\upsilon_{1/2} \approx 45$ Hz, 1 H), 51.45 ($\upsilon_{1/2} \approx 71$ Hz, 1 H), 51.61 ($\upsilon_{1/2} \approx 44$ Hz, 1 H), 57.56 ($\upsilon_{1/2} \approx 67$ Hz, 1 H), 63.61 ($\upsilon_{1/2} \approx 174$ Hz, 1 H), 67.96 ($\upsilon_{1/2} \approx 215$ Hz, 1 H), 81.49 ($\upsilon_{1/2} \approx 351$ Hz, 1 H), 86.69 ($\upsilon_{1/2} \approx 397$ Hz, 1 H), 103.50 ($\upsilon_{1/2} \approx 52$ Hz, 1 H), 117.53 ($\upsilon_{1/2} \approx 536$ Hz, 1 H), 128.64 ($\upsilon_{1/2} \approx 464$ Hz, 1 H). Anal. Calcd $H_{26}C_{23}N_3BrFe$: C, 57.52; H, 5.46; N, 8.75. Found: C, 58.17, 58.03; H, 5.61, 5.46; N, 8.42, 8.42. μ_{eff} (SQUID, 293 K) = 5.28 μ_B.

10. {κ-N,N$^{py}_2$-(2-pyridylmethyl)$_2$N(CH$_2$(4-^{t}Bu-phenyl-2-Br))}FeBr$_2$ (3-Fe). To a 25 mL round-bottom flask containing $FeBr_2$ (0.127 g, 0.59 mmol) and **BrArpy$_2$N** (0.250 g, 0.59 mmol) was vacuum transferred 10 mL of THF at −78 °C. The yellow suspension was warmed to 23 °C and darkened to orange-yellow after 1 h. The reaction mixture was stirred for 6 h, and the volatiles were removed. The yellow solid was taken up in Et_2O, filtered and washed to yield **3**-Fe (0.365 g, 97%). ^{1}H NMR (CD_2Cl_2, 400 MHz) δ: 0.84 ($\upsilon_{1/2} \approx 9$ Hz, C(C*H*$_3$)$_3$,9 H), 1.36 ($\upsilon_{1/2} \approx 37$ Hz, C*H*$_2$,2 H), 5.54 ($\upsilon_{1/2} \approx 39$ Hz, C*H*, 1 H), 6.21 ($\upsilon_{1/2} \approx 24$ Hz, C*H*, 1 H), 23.96 ($\upsilon_{1/2} \approx 425$ Hz, C*H*, 1 H), 27.18 ($\upsilon_{1/2} \approx 432$ Hz, py-C*H*, 2 H), 50.48 ($\upsilon_{1/2} \approx 51$ Hz, C*H*$_2$, 2 H), 55.80 ($\upsilon_{1/2} \approx 44$ Hz, C*H*$_2$, 2 H), 102.43 ($\upsilon_{1/2} \approx 417$ Hz, py-C*H*, 2 H), 105.92 ($\upsilon_{1/2} \approx 231$ Hz, py-C*H*, 2 H), 116.06 ($\upsilon_{1/2} \approx 461$ Hz, py-C*H*, 2 H). Anal. Calcd $H_{26}C_{23}N_3Br_3Fe$: C, 43.16; H, 4.09; N, 6.57. Found: C, 43.18, 42.95 H, 4.23, 4.05; N, 6.43, 6.37. μ_{eff} (Gouy balance, 295 K) = 4.5 μ_B.

11. Cr{N(TMS)$_2$}$_2$(THF)$_2$. A modified literature synthesis was used.[48] To a 250 mL flask charged with $CrCl_2$(THF) (5.325 g, 27.31 mmol) and sodium hexamethydisilazide (10.000 g, 54.53 mmol) was vacuum transferred 150 mL of THF at −78 °C. The reaction mixture immediately became a deep indigo and was slowly warmed to 23 °C. After stirring at 23 °C for 12 h, the reaction was filtered, yielding a lavender filtrate and a green filter cake that was washed with THF. The filtrates were concentrated, cooled to −78 °C, and filtered to yield 10.050 g of Cr{N(TMS)$_2$}$_2$(THF)$_2$ as a crystalline lavender solid (71%).

12. {κ-N,N$^{py}_2$-(1,3-dipyridyl-2-azaallyl}CrN(TMS)$_2$ ((smif)Cr-N(TMS)$_2$, 4-Cr). a. To a 25 mL round-bottom flask containing Cr{N(SiMe$_3$)$_2$}$_2$(THF)$_2$ (0.250 g, 0.48 mmol) and **BrArpy$_2$N** (0.206 g, 0.48 mmol) was vacuum transferred 15 mL of Et_2O at −78 °C. The reaction mixture immediately turned green and was slowly warmed to 23 °C. After stirring at 23 °C for 1 d, the volatiles were removed in vacuo. The green solid was filtered in pentane to yield (smif)CrN(SiMe$_3$)$_2$ as a green solid (0.103 g, 52%). **b.** A solution of (smif)H (0.153 g, 0.78 mmol) in 10 mL Et_2O was added dropwise to a stirred solution of Cr{N-(SiMe$_3$)$_2$}$_2$(THF)$_2$ (0.400 g, 0.77 mmol) in Et_2O (10 mL) at 23 °C. The solution became emerald green. The reaction was degassed and allowed to stir for 12 h at 23 °C while green crystals precipitated from solution. The suspension was concentrated, filtered, and washed with cold Et_2O to isolate 0.237 g **4**-Cr as green crystals (74%). ^{1}H NMR (C_6D_6, 400 MHz) δ: −78.71 ($\upsilon_{1/2} \approx 2000$ Hz, py-C*H*,1 H), −74.23 ($\upsilon_{1/2} \approx 300$ Hz, C*H*, 1 H), −37.81 ($\upsilon_{1/2} \approx 520$ Hz, py-C*H*, 1 H), −18.60 ($\upsilon_{1/2} \approx 580$ Hz, py-C*H*,1 H), 23.28 ($\upsilon_{1/2} \approx 500$ Hz, py-C*H*, 1 H), 57.60 ($\upsilon_{1/2} \approx 5800$ Hz, Si(C*H*$_3$)$_3$, 9 H). Anal. Calcd $H_{28}C_{18}N_4Si_2Cr$: C, 52.91; H, 6.91; N, 13.71. Found: C, 51.90; H, 6.78; N, 14.02. μ_{eff} (SQUID, 293 K) = 4.9 μ_B.

Magnetic Susceptibility Measurements. Magnetic susceptibility measurements of crystalline powdered samples (10−30 mg) were performed on a Quantum Design MPMS-5 SQUID magnetometer at 10 kOe between 5 and 300 K for all samples. All sample preparations and manipulations were performed under an inert atmosphere because of the air sensitivity of the samples. The samples were either measured in a flame-sealed NMR tube or a custom machined sealed Teflon capsule. The diamagnetic contribution from the sample container was subtracted from the experimental data. Pascal's constants[62] were used to subtract diamagnetic contributions, yielding paramagnetic susceptibilities.

Single Crystal X-ray Diffraction Studies. Upon isolation, the crystals were covered in polyisobutenes and placed under a 173 K N_2 stream on the goniometer head of a Siemens P4 SMART CCD area detector (graphite-monochromated Mo Kα radiation, λ = 0.71073 Å). The structures were solved by direct methods (SHELXS). All non-hydrogen atoms were refined anisotropically unless stated, and hydrogen atoms were treated as idealized contributions (Riding model).

13. 2-Fe. A red rod (0.20 × 0.03 × 0.03 mm) was obtained from toluene. A total of 15,951 reflections were collected with 3,192 determined to be symmetry independent (R_{int} = 0.1178), and 1,896 were greater than 2σ(I). A semiempirical absorption correction from equivalents was applied, and the refinement utilized $w^{-1} = \sigma^2(F_o^2) + (0.0499p)^2 + 0.0000p$, where $p = ((F_o^2 + 2F_c^2)/3)$.

14. 4-Cr. A dark green hexagonal block (0.40 × 0.30 × 0.20 mm) was obtained from pentane. A total of 7,678 reflections were collected with 7,678 determined to be symmetry independent (R_{int} = 0.0000), and 5,121 were greater than 2σ(I). A semiempirical absorption correction from equivalents was applied, and the refinement utilized $w^{-1} = \sigma^2(F_o^2) + (0.0400p)^2 + 0.0000p$, where $p = ((F_o^2 + 2F_c^2)/3)$.

Acknowledgment. We thank the National Science Foundation (CHE-0718030, PTW) and Cornell University for financial support. We thank Dr. Suzanne Doucette, and Dr. Susanne Mossin for obtaining SQUID data, and Dr. Karsten Meyer and Dr. Jay Winkler for helpful discussions.

Supporting Information Available: CIF files of **2**-Fe and **4**-Cr. This material is available free of charge via the Internet at http://pubs.acs.org.

(62) Carlin, R. L. *Magnetochemistry*; Springer-Verlag: Berlin; New York, 1986.